Electronic structure and lattice dynamics in the $FeSb_3$ skutterudite from density functional theory

Mikael Råsander,[1,*] Lars Bergqvist,[1,2] and Anna Delin[1,2,3]

[1]*Department of Materials and Nanophysics, KTH Royal Institute of Technology, Electrum 229, SE-164 40 Kista, Sweden*

[2]*SeRC (Swedish e-Science Research Center), KTH, SE-100 44 Stockholm, Sweden*

[3]*Department of Physics and Astronomy, Uppsala University, Box 516, SE-751 20 Uppsala, Sweden*

(Received 9 April 2014; revised manuscript received 27 October 2014; published 8 January 2015)

We have performed density functional calculations of the electronic structure and lattice dynamics of the binary skutterudite $FeSb_3$. We find that the ground state of $FeSb_3$ is a near half-metallic ferromagnet with $T_c = 175$ K. Furthermore, we find that $FeSb_3$ is softer than $CoSb_3$ based on an analysis of the relation of the elastic constants and the shape of the phonon density of states in the two systems, which is in agreement with experimental observation. Based on these observations we find it plausible that $FeSb_3$ will have a lower thermal conductivity than $CoSb_3$. Additionally, our calculations indicate that $FeSb_3$ may be stable towards decomposition into $FeSb_2$ and Sb. Furthermore, for ferromagnetic $FeSb_3$ we obtain real-valued phonon frequencies and also a c_{44} greater than zero, indicating that the system is mechanically as well as dynamically stable.

DOI: 10.1103/PhysRevB.91.014303 PACS number(s): 71.15.Mb, 63.20.−e

I. INTRODUCTION

The skutterudites constitute an interesting class of materials for applications as thermoelectric energy converters [1], since they possess the necessary electronic properties, notably a large Seebeck coefficient, and a low thermal conductivity. The latter is largely due to filler atoms that occupy large voids in the crystal structure [2–7]. The exact mechanism of the filler atoms to lower the thermal conductivity is debated [8]. The skutterudites can generally be presented as $R_yM_4X_{12}$, where M is a transition metal, such as Co, Ir, and Rh. X is a pnictogen, e.g., P, As, and Sb, and R is the filler atom, typically a rare-earth element, such as La or Ce. The skutterudites offer many possibilities for engineering in order to optimize their properties by alloying on the metal or pnictogen lattices, as well as by careful selection of the filler element.

$CoSb_3$ is an archetypical skutterudite system. It has excellent electronic properties and especially it has a high Seebeck coefficient [9–13]. Unfortunately, the thermal conductivity of $CoSb_3$ is too large to give a high thermoelectric efficiency. The ability to lower the thermal conductivity in $CoSb_3$ by using filler atoms is limited [14] since the filling factor y is rather small and focus on filled skutterudites has rather been directed towards other skutterudites such as Fe containing $R_yFe_xCo_{1-x}Sb_{12}$. For these systems the filling factor is larger and for $R_yFe_4Sb_{12}$ the filling factor reaches unity [2–6]. Filled $R_yFe_4Sb_{12}$ systems have been studied for quite some time. However, the binary $FeSb_3$ system has not received much attention even though an understanding of the dynamics of the filler and its impact on the electronic structure and thermal conductivity cannot be complete without an understanding of the properties of the host framework. According to the phase diagram [15] $FeSb_3$ is metastable in comparison to $FeSb_2$ and Sb. Recently, however, micrometer thick films of $FeSb_3$ have been synthesized by nanoalloying of Fe and Sb precursors at $T \sim 400$ K [16,17] and their physical properties investigated experimentally [17]. A significant difference compared to $CoSb_3$ is that $FeSb_3$ is softer and a softening of low-energy phonon modes would likely have a favorable influence towards a lower thermal conductivity of $FeSb_3$ compared to $CoSb_3$.

Since there are no theoretical studies focusing on $FeSb_3$ we investigate the electronic structure, lattice dynamics, and possible dynamic stability of $FeSb_3$ using methods based on density functional theory. We compare our results with calculations for the well-known $CoSb_3$ system in order to elucidate the differences between these two superficially rather similar compounds. In addition, we will analyze how filling the voids in $FeSb_3$ with La affects the lattice dynamics.

The paper is outlined as follows: In Sec. II we will present the details of our calculations and in Sec. III we will present our results. Finally in Sec. IV we will summarize our findings and present our conclusions.

II. COMPUTATIONAL DETAILS

The binary skutterudite structure has a unit cell containing four formula units with body centered cubic lattice vectors and belongs to the space group $Im\bar{3}$ (No. 204), where metal atoms and pnictogen atoms occupy the $8c$ and $24g$ positions, respectively. The pnictogen atoms occupy the general position $(0,y,z)$ and these values along with our calculated lattice constants are shown in Table I. The skutterudite framework, i.e., MX_3, contains large voids at the $2a$ positions of the lattice. Filling these voids by other atoms does not change the symmetry of the crystal. In Fig. 1 we show the conventional unit cell of the skutterudite structure (8 formula units) with the voids, at (0,0,0) and $(\frac{1}{2},\frac{1}{2},\frac{1}{2})$, filled with a rare-earth element. The structure can also be viewed as consisting of eight cubes made up of metal atoms. Six of these cubes are filled with almost square planar "rings" of pnictogen atoms, which are oriented parallel to one of the unit cell edges. The two nearest neighbor pnictogen to pnictogen binding distances are therefore d_1 and d_2 along the edges of the rings. These will be identical if $y + z = 1/2$. In this study the rare-earth element is La, and calculations have been performed for the $FeSb_3$ and $CoSb_3$ binary skutterudites and the filled $LaFe_4Sb_{12}$.

Density functional calculations have been performed using the projector augmented wave (PAW) method [18] as it is implemented in the Vienna *ab initio* simulation package

*mikael.rasander@gmail.com

TABLE I. Comparison of the evaluated lattice constants and crystallographic y and z values for the Sb atoms in $FeSb_3$ for spin-polarized [in ferromagnetic (FM) and anti-ferromagnetic (AFM) configurations] and non-spin-polarized (NSP) calculations. The Vegard's law value is extracted from a study on $Co_{1-x}Fe_xSb_3$ with $x \leqslant 0.1$ [26].

System		a (Å)	y	z
$FeSb_3$	NSP	9.153	0.327	0.160
$FeSb_3$	FM	9.178	0.331	0.160
$FeSb_3$	AFM	9.166	0.331	0.159
$FeSb_3$	Expt. [16]	9.176	0.340	0.162
$FeSb_3$	Expt. ($T = 10$ K) [17]	9.212	0.340	0.158
$FeSb_3$	Expt. ($T = 300$ K) [17]	9.238	0.340	0.157
$FeSb_3$	Vegard's law [26]	9.126	–	–
$CoSb_3$	NSP	9.115	0.333	0.160
$CoSb_3$	Expt. [27]	9.039	0.335	0.158
$LaFe_4Sb_{12}$	NSP	9.181	0.335	0.164
$LaFe_4Sb_{12}$	FM	9.186	0.335	0.163
$LaFe_4Sb_{12}$	Expt. [28]	9.142	0.354	0.150

(VASP) [19,20]. The generalized gradient approximation due to Perdew, Burke, and Ernzerhof (PBE) [21] has been used for the exchange-correlation energy functional. Relaxation of the ionic position as well as the volume of the systems have been performed until the forces on individual atoms were smaller than 0.1 meV/Å. A k-point mesh of $12\times12\times12$ [22] was found to be accurate enough for obtaining converged total energies and structural parameters. The plane wave energy cutoff was set to 600 eV. Spin polarization was considered for all systems and it will be made clear when a non-spin-polarized (NSP), ferromagnetic (FM) or antiferromagnetic (AFM) solution is discussed. Effects due to spin-orbit coupling (SOC) have been investigated for $FeSb_3$ and $CoSb_3$. In general, as will be presented, these effects are small.

We focus here on the electronic structure and lattice dynamics of the $FeSb_3$ system in relation to the more studied $CoSb_3$ and $LaFe_4Sb_{12}$ systems. However, we have accurately calculated the Curie temperature (T_c) of $FeSb_3$ by calculating the exchange parameters within a Heisenberg model using the SPR-KKR package [23], where the crystal geometry was taken from our PAW calculations, and subsequent Monte Carlo simulations using the UPPASD package [24].

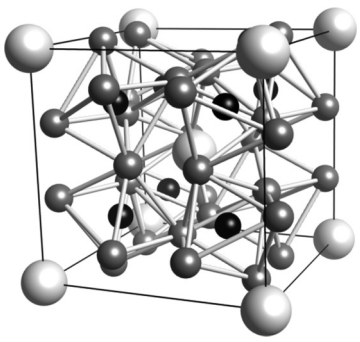

FIG. 1. Illustration of the crystal structure of the skutterudite structure. Fe (black spheres) is residing inside canted octahedral cages of Sb (gray spheres). Filler atoms are presented by large white spheres. In this case the filler is La.

The lattice dynamics have been calculated within the harmonic approximation at $T = 0$ K by means of the small displacement method, as it is implemented in the PHONOPY code [25]. The results shown here are obtained for a $3\times3\times3$ multiplication of the primitive skutterudite unit cell which is considered large enough to yield well-converged lattice dynamical properties. The size of the displacements was 0.01 Å. For the supercells a $2\times2\times2$ k-point mesh has been used for the electronic structure calculations from which the forces acting on the atoms have been evaluated. In the calculations of the phonon density of states (PDOS) a $20\times20\times20$ q-point mesh has been utilized.

III. RESULTS

A. Structural properties and phase stability

In Table I we show the evaluated structural parameters for $FeSb_3$, $CoSb_3$, and $LaFe_4Sb_{12}$. We find that the non-spin-polarized (NSP) calculation for $FeSb_3$ yields a smaller lattice constant compared to the result obtained by ferromagnetic (FM) and antiferromagnetic (AFM) calculations. The y and z coordinates are, however, similar in all three cases, especially so for the z coordinate. Compared to experiments there is a very good agreement in the lattice constant between the FM calculation and the experiment by Hornbostel *et al.* [16], while for the lattice constant obtained by Möchel *et al.* [17] the difference is larger. Even so, the discrepancy is smaller than 1%. Both of the experimental studies on $FeSb_3$ also find $y = 0.340$ which is larger than our value of 0.331. However, the z values are very similar. Compared to $CoSb_3$ the Fe-containing system has a larger lattice constant, while the y and z values are very similar in our calculations. When filling the voids in $FeSb_3$ with La, we find that the lattice constant increases by ~0.03 Å in the case of NSP calculations and by ~0.01 Å in the case of FM calculations, which means that incorporation of La into the lattice is made easier for the FM system. Available experimental data, shown in Table I, suggest that incorporating La into $FeSb_3$ causes the lattice to shrink by 0.034 Å or 0.070 Å depending on which study is used for the lattice constant of $FeSb_3$. A study on $Co_{1-x}Fe_xSb_3$ for small values for x has revealed a linear dependence of the lattice constant with increasing Fe content indicative of a Vegard's law behavior [26]. According to this trend the lattice constant for $FeSb_3$ would be 9.126 Å. This is significantly smaller than the experimental observations for $FeSb_3$ of 9.176 Å [16] and 9.212 Å [17]. We note that in the case of $CoSb_3$ and $LaFe_4Sb_{12}$ our calculations give lattice constants that are larger than experiments by 0.076 Å and 0.044 Å, respectively (see Table I). In the case of FM $FeSb_3$ our result is 0.052 Å larger than the Vegard's law value of 9.126 Å. If the experimental lattice constant would be more in line with the Vegard's law value we find a similar overestimation of the lattice constants in $FeSb_3$, $CoSb_3$, and $LaFe_4Sb_{12}$, in agreement with the usual tendency of GGA approximations to overestimate the lattice constants by a few percent. Additionally, a smaller value for the lattice constants would suggest that the $FeSb_3$ lattice increases when La is introduced into the voids in agreement with our calculations.

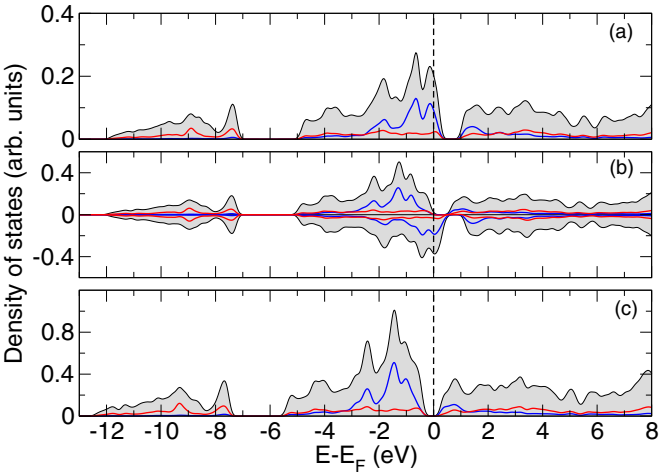

FIG. 2. (Color online) Calculated density of states (DOS) of NSP $FeSb_3$ (a), FM $FeSb_3$ (b), and $CoSb_3$ (c). In (b) the positive DOS is for the spin-up channel and the negative valued DOS is for the spin-down channel. The vertical dashed lines mark the position of the Fermi level. Projected DOS onto Fe(Co) and Sb atoms are represented by blue and red curves, respectively.

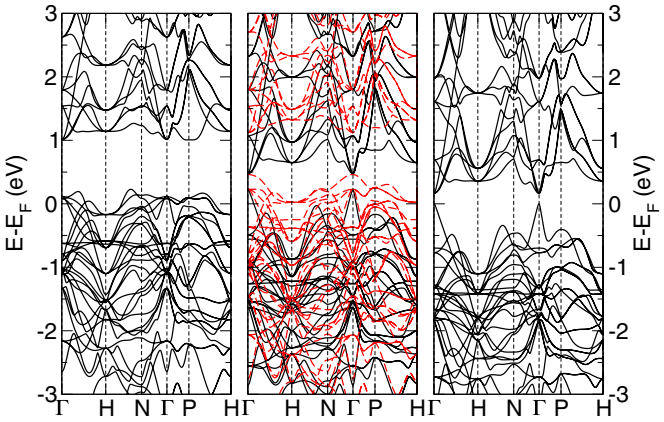

FIG. 3. (Color online) Calculated band structures along high symmetry directions in the Brillouin zone of NSP $FeSb_3$ (left panel), FM $FeSb_3$ (middle panel), and $CoSb_3$ (right panel). In the middle panel the spin-up bands are plotted with solid (black) lines and the spin-down bands are plotted with dashed (red) lines. The zero on the energy scale is the Fermi level E_F.

In addition, we have calculated the energy of the $FeSb_3$ phase in relation to $FeSb_2$ and elemental Sb according to $\Delta E = E(FeSb_3) - E(FeSb_2) - E(Sb)$, where $E(X)$ is the total energy of system X with X = $FeSb_3$, $FeSb_2$, and Sb. Here, $FeSb_2$ has been evaluated in its orthorhombic ground state with the space group Pnn2 (No. 34), while Sb has been calculated in the A7-type structure with space group $R\bar{3}mh$ (No. 166). We have used FM $FeSb_3$, NSP $FeSb_2$, and NSP Sb as reference states in these calculations. The resulting very small energy difference of -0.02 eV/f.u. suggests that the $FeSb_3$ phase may be stable or nearly stable towards decomposition into $FeSb_2$ and elemental Sb. Note that these energies are normalized per formula unit, f.u., of $FeSb_3$. If SOC is included $\Delta E = -0.01$ eV/f.u.

B. Electronic structure

In Fig. 2 we show the electronic density of states (DOS) of NSP $FeSb_3$, FM $FeSb_3$, and $CoSb_3$. The corresponding band structures are shown in Fig. 3. It is clear that NSP $FeSb_3$ is a metal with a large DOS at the Fermi level E_F. The DOS also contains a gap between the valence band edge and higher lying conduction bands. Furthermore, the electronic properties of $FeSb_3$ are very different from $CoSb_3$, which is a semiconductor with a small direct gap at the Γ point of about 0.17 eV in agreement with previous theory [10]. The large DOS at the Fermi level in the NSP $FeSb_3$ makes it energetically favorable for the system to form a ferromagnetic ground state, which can be deduced from the Stoner criterion, i.e., $N(E_F)I > 1$, where $N(E_F)$ is the DOS at the Fermi level and I is the Stoner exchange parameter. FM $FeSb_3$ can be described as a near half-metal, where the spin-up channel is almost completely filled with a direct gap at the Γ point of about 0.26 eV. The spin-down channel has a significant DOS at the Fermi level and up to about 0.5 eV above the Fermi level where a gap of about 0.7 eV is found to the conduction bands at higher energies.

In $CoSb_3$ the Sb states are distributed on both sides of the Fermi level rather evenly, both in the lower, between -13 eV and -7.5 eV, and upper, between -5.5 eV and the Fermi level, valence band regions, as well as in the conduction bands. The Co d states are positioned just below the Fermi level. In NSP $FeSb_3$ the Fermi level has moved down into the upper valence band region into a region with a large density of Fe states. The large number of states at the Fermi level is, as already mentioned above, the cause for the stabilization of the FM state. In FM $FeSb_3$, the spin-up DOS has the Fe states positioned below the Fermi level, while the spin-down channel has the Fermi level in a region of large DOS. $CoSb_3$ and NSP $FeSb_3$ have DOS that is very similar.

Based on the DOS, it is easy to analyze the DOS of NSP $FeSb_3$ within a rigid band model as $CoSb_3$ with one less electron per metal atom. However, when analyzing the band structures in Fig. 3, this is no longer true. It is clear that there are important differences in the electronic structure of $FeSb_3$ and $CoSb_3$. In $CoSb_3$ the highest valence band sticks out above the other bands at the Γ point with a quadratic dispersion close to Γ that turns into a linear dispersion which extends far out into the Brillouin zone, especially along Γ to H [9]. This band has p character and is responsible for the large Seebeck coefficient found in this material [9]. The corresponding band, with similar features, is also found in $FeSb_3$, however, for the NSP $FeSb_3$ it is coexisting with several bands with small dispersion, mostly derived from Fe d states, which give rise to the large DOS at the Fermi level. For FM $FeSb_3$ the same band is found in the spin-up channel, however, there are several spin-down bands with large Fe d character at the same energy. It is clear from Fig. 3 that the spin-up channel has a not completely full valence band and the system is therefore close to being a half-metal. A small electron doping to the system would make $FeSb_3$ into a half-metal.

In Fig. 4, we show the calculated band structures of Fig. 3 close to the Fermi level. In addition, we have in this figure added the result with SOC included in the calculations. With SOC, we find the typical lifting of degeneracies. For example, the triply degenerate lowest conduction band at the Γ point in $CoSb_3$ changes into a doubly degenerate state and a singlet

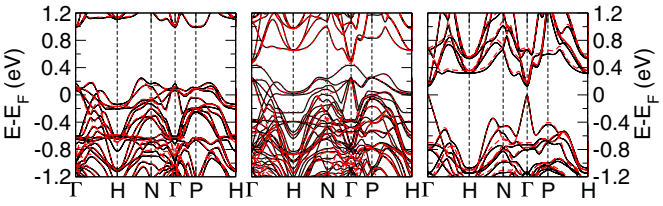

FIG. 4. (Color online) Calculated band structures including SOC along high symmetry directions in the Brillouin zone of NSP $FeSb_3$ (left panel), FM $FeSb_3$ (middle panel), and $CoSb_3$ (right panel). Band structures including SOC is given in black. The band structures obtained without SOC are given with dashed red lines. In the middle panel the spin-down channel is given by the dotted red line. The zero on the energy scale is the Fermi level E_F.

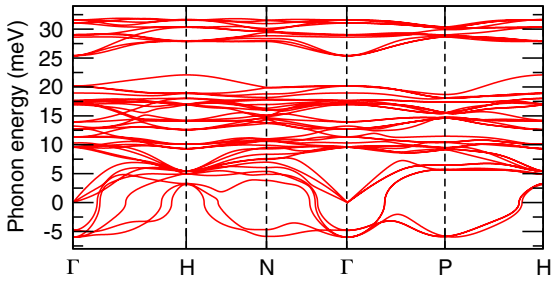

FIG. 5. (Color online) The resulting phonon dispersions along high symmetry directions in the Brillouin zone based on a non-spin-polarized density functional calculation of $FeSb_3$. Imaginary phonon energies are plotted with negative values. Note the imaginary phonon energies along all directions shown.

state. In addition, we find that the inclusion of SOC makes the band gap in $CoSb_3$ slightly smaller. Otherwise the effect of SOC is small on the overall features of the electronic structure as witnessed by the band structures in Fig. 4.

The magnetic moments in the FM and AFM calculations are to a large extent localized on the Fe atoms, with a magnetic moment of $\sim$1.0 μ_B/Fe and $\sim$1.1 μ_B/Fe, respectively. The same is true for FM $LaFe_4Sb_{12}$, however, for this system the magnetic moment on the Fe has dropped to $\sim$0.3 μ_B/Fe. We also find small induced moments on the Sb atoms (less than 0.01 μ_B/atom) and on the La ($\sim$0.05 μ_B) in the opposite direction to the moments localized on the Fe atoms. The magnetization energy, i.e., the energy between the FM (or AFM) and the NSP calculations, is for $FeSb_3$ -0.28 eV (FM) and -0.13 eV (AFM), which suggests that FM $FeSb_3$ is the ground state. For this state, we obtained a Curie temperature of 175 K which is well below the relevant thermoelectric operating temperatures. In the case of $LaFe_4Sb_{12}$ the magnetization energy has been lowered to -0.02 eV which is very small and throughout the remainder of the paper we will only consider NSP $LaFe_4Sb_{12}$. As expected, $CoSb_3$ shows no tendency for a magnetic solution. We note that $FeSb_3$ filled with the alkali metals Na and Ca has previously been found to result in ferromagnetic systems [7].

C. Elastic constants and the velocity of sound

In Table II we show the calculated elastic constants of $FeSb_3$ and $CoSb_3$. We find that essentially all elastic constants are smaller in $FeSb_3$ compared to $CoSb_3$. It is only c_{12} that is larger in $FeSb_3$, although the differences in the c_{12} in the two systems are small. The bulk modulus B and the tetragonal shear constant c' are both larger in $CoSb_3$ compared to $FeSb_3$. We can therefore conclude that the $FeSb_3$ framework is softer than $CoSb_3$, which is in agreement with experimental findings [17] as well as with our analysis of the lattice dynamics (see below). Möchel *et al.* [17] have reported the bulk modulus of $FeSb_3$ to be 47.9(1) GPa [17] which is much smaller than the values obtained by us here. For $CoSb_3$ the experimental bulk modulus is 83.2(1) GPa [17] which is in excellent agreement with our result. We note that in their study Möchel *et al.* [17] determined the bulk modulus in $FeSb_3$ with the assumption that the Poisson's ratio in $FeSb_3$ is identical to the value in $CoSb_3$.

TABLE II. Calculated elastic constants of NSP, FM, and AFM $FeSb_3$ in comparison to $CoSb_3$ calculated according to Refs. [30,31]. $B = (1/3)(c_{11} + 2c_{12})$ is the bulk modulus and $c' = (1/2)(c_{11} - c_{12})$ is the tetragonal shear constant.

System	c_{11} (GPa)	c_{12} (GPa)	c_{44} (GPa)	B (GPa)	c' (GPa)
NSP	166.0	41.7	22.0	83.1	62.2
FM	166.0	37.1	35.0	80.1	64.5
AFM	156.6	37.0	31.6	76.9	59.8
$CoSb_3$	181.8	36.5	49.4	84.9	72.7

The difference in the size of the elastic constants will affect the velocity of sound in the materials, since the latter in a given direction is given by $c = \sqrt{c_{\text{eff}}/\rho}$, where c_{eff} is a linear combination of elastic constants depending on the direction and ρ is the mass density of the material. A simple analysis yields that the increased stiffness of $CoSb_3$ compared to $FeSb_3$ means that sound waves travel more readily in $CoSb_3$. Since the velocity of sound is in turn related to the thermal conductivity of the material we may anticipate that the thermal conductivity is lower in $FeSb_3$ compared to $CoSb_3$. However, this has to be supported in a more rigorous fashion.

D. Lattice dynamics

In Fig. 5 we show the calculated phonon dispersion energies of NSP $FeSb_3$. Several phonon modes have imaginary phonon energies and it is clear that NSP $FeSb_3$ is dynamically unstable within the harmonic approximation. By allowing for an FM solution this behavior will change and all phonon modes will have real values. This is shown in Fig. 6, where we present the calculated phonon energy dispersions of FM $FeSb_3$ and compare these with the results obtained for $CoSb_3$ and $LaFe_4Sb_{12}$. For the remainder of the paper we will focus only on FM $FeSb_3$ and the FM descriptor will be omitted throughout.

In Fig. 6, it is clear that the phonon modes can be divided into two regions in terms of energy: The lower region which contains both acoustic and optical modes, which in the case of $FeSb_3$ lies in the energy range of 0–20 meV, and the upper optical region, which for $FeSb_3$ lies in between 27 and 33 meV. In $CoSb_3$ the lower region reaches $\sim$25 meV which is about 5 meV higher in energy compared to $FeSb_3$. This suggests

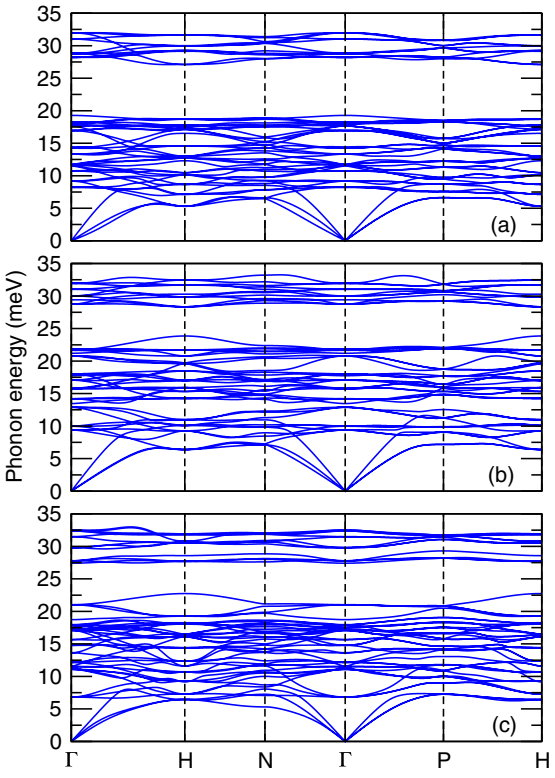

FIG. 6. (Color online) Calculated phonon dispersions for (a) FM $FeSb_3$, (b) $CoSb_3$, and (c) $LaFe_4Sb_{12}$ along high symmetry directions in the Brillouin zone.

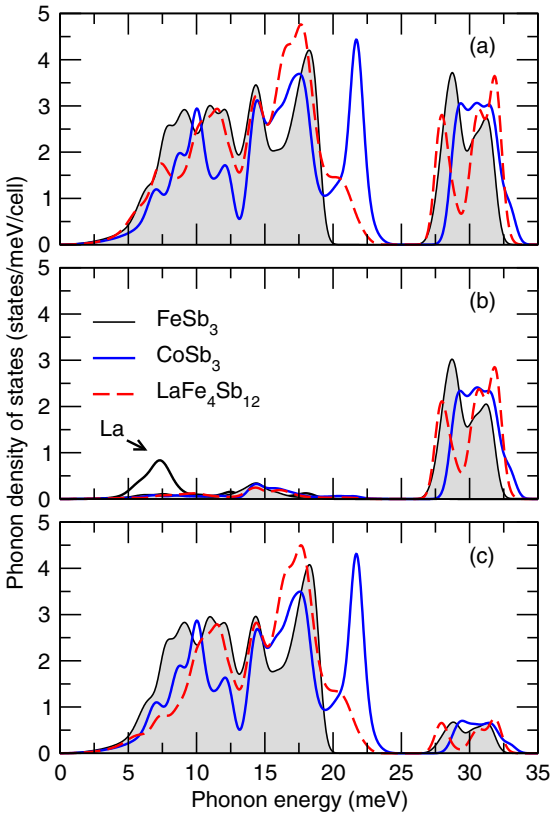

FIG. 7. (Color online) Phonon density of states (PDOS) of $FeSb_3$, $CoSb_3$, and $LaFe_4Sb_{12}$, (a) total PDOS, (b) projected PDOS on metallic species, i.e., Fe, Co, and La, (c) projected PDOS on Sb. The projected PDOS onto La is given by the thick black line in (b). For clarity, the PDOS on atoms in the $FeSb_3$ system are shaded in gray. Note that the unit is states/meV/cell, where the cell is either Fe_4Sb_{12}, Co_4Sb_{12} or $LaFe_4Sb_{12}$.

that $FeSb_3$ is softer than $CoSb_3$ which agrees well with recent experimental findings [17]. Furthermore, there is a gap at about 13 meV in the phonon dispersions of $CoSb_3$ which splits the lower phonon energy region. Among the systems studied here, this gap is unique to $CoSb_3$. The existence of this gap has been observed previously by both theory and experiment [2–6]. A similar split is found in the upper optical region in $LaFe_4Sb_{12}$ with a gap at 27 meV, which is dramatically different from the behavior in the binary systems where this region contains modes with dispersions that cross and overlap each other. In $LaFe_4Sb_{12}$ we also note a clear signature of avoided crossing [29] of the acoustic and low lying optical modes along the line connecting Γ and P which does not exist in the binary systems. The acoustic phonon modes are also found to be nondegenerate along most directions in the Brillouin zone. It is only along Γ to P where the two lowest energy phonon modes are degenerate for all three systems in our study.

In Fig. 7 we present the total and projected phonon density of states (PDOS) for $FeSb_3$, $CoSb_3$, and $LaFe_4Sb_{12}$. In $FeSb_3$ the lower energy region between 0 and 20 meV is dominated by Sb and the upper region between 27 and 33 meV is dominated by Fe. We find that the PDOS of Fe has two small broad peaks at ∼7 meV and ∼15 meV, as well as a larger feature between 27 and 33 meV which has two clear peaks [see Fig. 7(b)]. The Sb projected PDOS is more or less flat between 0 and 20 meV with two valleys at ∼13 meV and ∼16 meV. Additionally, there is a peak at about 18 meV in the Sb PDOS. These observations are in good agreement with available experimental PDOS measured by Möchel *et al.* [17] Compared to $CoSb_3$, also plotted in Fig. 7, the PDOS of $FeSb_3$ show the same behavior as the phonon dispersions, namely that the lower phonon energy region is narrower in $FeSb_3$.

In $CoSb_3$ the Sb projected PDOS shows distinct features, such as two deep valleys at ∼13 meV and ∼20 meV as well as a very distinct peak at ∼22 meV. The very deep valley at 13 meV coincides with the gap in the phonon dispersions for $CoSb_3$ shown in Fig. 6. Comparing the position of the peak at 22 meV in the PDOS with the same energy region in the phonon dispersions in Fig. 6 we note that at this energy the phonon modes show a very small degree of dispersion which leads to a high PDOS at this energy. In $FeSb_3$ this feature has moved towards lower energies and the peak in the PDOS is found at about 18 meV. The valley in the Sb PDOS of $CoSb_3$ at 20 meV corresponds to a region with a relatively large dispersion of the phonon modes which results in a lower PDOS. The similar region in $FeSb_3$ can be found at about 15 meV.

For the PDOS projected onto Co we find that it also shows smaller features at the same energies as the Fe PDOS in $FeSb_3$, however, the feature at large phonon energies is shifted to slightly larger energies for the Co PDOS compared to the case of Fe in $FeSb_3$, and this feature is flat which is a distinct difference to Fe in $FeSb_3$. The two binary skutterudite systems therefore show distinct differences in their lattice dynamics and especially so for the dynamics of the Sb atoms in the two

systems. The behavior of the phonon modes depends on the size of the force constants in a material and these are smaller in $FeSb_3$ compared to $CoSb_3$, especially so for the Sb-Sb force constants within the planar Sb rings. The conclusion is that $FeSb_3$ is softer than $CoSb_3$.

When La is inserted into $FeSb_3$, we find that the total PDOS from 0 up to about 7.5 meV are very similar, however, when projected onto Sb there is a marked difference between the filled and unfilled systems in this region. The Sb PDOS has been reduced in response to the filling in this region. This reduction in the Sb PDOS for $LaFe_4Sb_{12}$ coincides with the appearance of a filler mode due to vibrations of the La centered around 7 meV (see Fig. 7). We also find a shoulder in the Sb PDOS for the filled system at this energy which suggests that the La and Sb vibrations are connected and not independent which is in agreement with experimental observations [8]. In addition to the large La peak at about 7 meV, we find smaller features due to the filler in the La PDOS at about 12.5 and 18 meV in agreement with previous theory and experiment [2]. Furthermore, we find that the PDOS of the filled system is broadened compared to the unfilled $FeSb_3$, with a marked shoulder beginning at 20 meV, and that the Fe PDOS region at high phonon energies are split with a deep valley at just below 30 meV. This latter feature is due to the gap in the high energy optical modes which is clearly visible in Fig. 6.

IV. SUMMARY AND CONCLUSIONS

We have performed density functional calculations on the $FeSb_3$ skutterudite system and analyzed its electronic structure and lattice dynamics. The electronic structure has been compared in detail with $CoSb_3$ while for the lattice dynamics comparison has also been done with the filled $LaFe_4Sb_{12}$ skutterudite phase. We find that $FeSb_3$ is a near half-metal with a ferromagnetic ground state and a Curie temperature of 175 K. The NSP $FeSb_3$ is a metal with a large DOS at the Fermi level which facilitates the ferromagnetic ground state.

We find that in order to obtain a dynamically stable system it is required to evaluate the lattice dynamics for the FM ground state of $FeSb_3$. Phonon calculations for the NSP phase yield unstable phonon modes along most high symmetry directions. We note that the calculations of the lattice dynamics have been done within the harmonic approximation at $T = 0$ K. However, the harmonic approximation is known to fail for systems that are stabilized at finite temperatures, since anharmonic effects are not included in the calculation. Famous examples are the high temperature phases of Zr [32,33], Ti [33], and Hf [33] which all have the bcc structure at elevated temperatures even though the bcc structure for these systems is dynamically unstable in the harmonic approximation. The low T_c for $FeSb_3$ combined with the fact that the phase is made experimentally at ∼400 K [16,17] suggest that the NSP phase will be stabilized at finite temperatures in a similar fashion as the examples mentioned above.

Compared to $CoSb_3$ we find that the lattice dynamics in $FeSb_3$ differs in several respects. For example, the Sb PDOS in $FeSb_3$ is more flat and narrower compared to $CoSb_3$ which shows more features in the PDOS. In addition, the PDOS of Fe at large phonon energies show a clear two peak feature which is not the case in $CoSb_3$ which is more flat. Primarily, we find that $FeSb_3$ is softer than $CoSb_3$ based on the form of the phonon energy dispersions and PDOS as well as from calculations of the elastic constants of the two systems.

When comparing $FeSb_3$ to filled $LaFe_4Sb_{12}$, we find a hardening at low phonon energies for the filled system of the Sb PDOS which coincides with the La PDOS peak centered at 7 meV. This hardening of the Sb PDOS is in perfect agreement with the experimental result of Möchel *et al.* [17].

Furthermore, we find that $FeSb_3$ is mechanically stable, i.e., has B, c', and c_{44} greater than zero, as well as dynamically stable in its bulk form. This suggests that it should be, in principle, possible for a process route to be established in order to produce bulk samples of binary $FeSb_3$.

ACKNOWLEDGMENTS

This work was financed through the EU project NexTec, VR (the Swedish Research Council), and SSF (Swedish Foundation for Strategic Research). The computations were performed on resources provided by the Swedish National Infrastructure for Computing (SNIC) at the National Supercomputer Centre in Linköping (NSC).

[1] G. J. Snyder and E. S. Toberer, Nat. Mater. **7**, 105 (2008).
[2] J. L. Feldman, P. Dai, T. Enck, B. C. Sales, D. Mandrus, and D. J. Singh, Phys. Rev. B **73**, 014306 (2006).
[3] J. L. Feldman and D. J. Singh, Phys. Rev. B **53**, 6273 (1996).
[4] J. L. Feldman and D. J. Singh, Phys. Rev. B **54**, 712E (1996).
[5] R. P. Hermann, R. Jin, W. Schweika, F. Grandjean, D. Mandrus, B. C. Sales, and G. J. Long, Phys. Rev. Lett. **90**, 135505 (2003).
[6] G. S. Nolas and C. A. Kendziora, Phys. Rev. B **59**, 6189 (1999).
[7] A. Leithe-Jasper, W. Schnelle, H. Rosner, M. Baenitz, A. Rabis, A. A. Gippius, E. N. Morozova, H. Borrmann, U. Burkhardt, R. Ramlau, U. Schwarz, J. A. Mydosh, Y. Grin, V. Ksenofontov, and S. Reiman, Phys. Rev. B **70**, 214418 (2004).
[8] M. M. Koza, M. R. Johnson, R. Viennois, H. Mutka, L. Girard, and D. Ravot, Nat. Mater. **7**, 805 (2008).
[9] D. J. Singh and W. E. Pickett, Phys. Rev. B **50**, 11235 (1994).
[10] D. Wee, B. Kozinsky, N. Marzari, and M. Fornari, Phys. Rev. B **81**, 045204 (2010).
[11] J. C. Smith, S. Banerjee, V. Pardo, and W. E. Pickett, Phys. Rev. Lett. **106**, 056401 (2011).
[12] V. Pardo, J. C. Smith, and W. E. Pickett, Phys. Rev. B **85**, 214531 (2012).
[13] L. Hammerscmidt, S. Schlecht, and B. Paulus, Phys. Status Solidi A **210**, 131 (2013).
[14] X. Shi, W. Zhang, L. D. Chen, and J. Yang, Phys. Rev. Lett. **95**, 185503 (2005).
[15] T. B. Massalski, H. Okamoto, P. R. Subramanian, and L. Kacpruk, eds., in *Binary Alloy Phase Diagrams*, 2nd ed. (ASM International, Metals Park, 1990), Vol. 2, pp. 2664–2665.

[16] M. D. Hornbostel, E. J. Hyer, J. Thiel, and D. C. Johnson, J. Am. Chem. Soc. **119**, 2665 (1997).
[17] A. Möchel, I. Sergueev, N. Nguyen, G. J. Long, F. Grandjean, D. C. Johnson, and R. P. Hermann, Phys. Rev. B **84**, 064302 (2011).
[18] P. E. Blöchl, Phys. Rev. B **50**, 17953 (1994).
[19] G. Kresse and J. Furthmüller, Phys. Rev. B **54**, 11169 (1996).
[20] G. Kresse and D. Joubert, Phys. Rev. B **59**, 1758 (1999).
[21] J. P. Perdew, K. Burke, and M. Ernzerhof, Phys. Rev. Lett. **77**, 3865 (1996).
[22] H. J. Monkhorst and J. D. Pack, Phys. Rev. B **13**, 5188 (1976).
[23] H. Ebert, D. Ködderitzsch, and J. Minar, Rep. Prog. Phys. **74**, 096501 (2010).
[24] B. Skubic, J. Hellsvik, L. Nordström, and O. Eriksson, J. Phys.: Condens. Matter **20**, 315203 (2008).
[25] A. Togo, F. Oba, and I. Tanaka, Phys. Rev. B **78**, 134106 (2008).
[26] J. Yang, G. P. Meisner, D. T. Morelli, and C. Uher, Phys. Rev. B **63**, 014410 (2000).
[27] T. Schmidt, G. Kliche, and H. D. Lutz, Acta Cryst. C **43**, 1678 (1987).
[28] R. Viennois, S. Charar, D. Ravot, A. Mauger, P. Haen, and J. C. Tédenac, J. Phys.: Condens. Matter **18**, 5371 (2006).
[29] E. S. Toberer, A. Zevalkink, and G. J. Snyder, J. Mater. Chem. **21**, 15843 (2011).
[30] Y. Le Page and P. Saxe, Phys. Rev. B **65**, 104104 (2002).
[31] X. Wu, D. Vanderbilt, and D. R. Hamann, Phys. Rev. B **72**, 035105 (2005).
[32] O. Hellman, I. A. Abrikosov, and S. I. Simak, Phys. Rev. B **84**, 180301 (2011).
[33] P. Souvatzis, O. Eriksson, M. I. Katsnelson, and S. P. Rudin, Phys. Rev. Lett. **100**, 095901 (2008).